Published in final edited form as:
Nat Neurosci. ; 14(10): 1253–1259. doi:10.1038/nn.2908.

Ligand-binding domain of an α_7-nicotinic receptor chimera and its complex with agonist

Shu-Xing Li[1,5], **Sun Huang**[2,5], **Nina Bren**[2,5], **Kaori Noridomi**[1], **Cosma D Dellisanti**[1], **Steven M Sine**[2,3], and **Lin Chen**[1,4]

[1]Molecular and Computational Biology, Departments of Biological Sciences and Chemistry, University of Southern California, Los Angeles, California, USA

[2]Department of Physiology and Biomedical Engineering Mayo Clinic College of Medicine, Rochester, Minnesota, USA

[3]Department of Neurology, Mayo Clinic College of Medicine, Rochester, Minnesota, USA

[4]Norris Comprehensive Cancer Center, Keck School of Medicine, University of Southern California, Los Angeles, California, USA

Abstract

The α_7 acetylcholine receptor (AChR) mediates pre- and postsynaptic neurotransmission in the central nervous system and is a potential therapeutic target in neurodegenerative, neuropsychiatric and inflammatory disorders. We determined the crystal structure of the extracellular domain of a receptor chimera constructed from the human α_7 AChR and *Lymnaea stagnalis* acetylcholine binding protein (AChBP), which shares 64% sequence identity and 71% similarity with native α_7. We also determined the structure with bound epibatidine, a potent AChR agonist. Comparison of the structures revealed molecular rearrangements and interactions that mediate agonist recognition and early steps in signal transduction in α_7 AChRs. The structures further revealed a ring of negative charge within the central vestibule, poised to contribute to cation selectivity. Structure-guided mutational studies disclosed distinctive contributions to agonist recognition and signal transduction in α_7 AChRs. The structures provide a realistic template for structure-aided drug design and for defining structure–function relationships of α_7 AChRs.

Nicotinic AChRs mediate rapid excitatory synaptic transmission in the brain and periphery. An essential step toward understanding the mechanisms behind AChR-mediated excitation is determining AChR structure. X-ray crystal structures of the related AChBP revealed the overall fold of the extracellular domain of the subunits and positioning of subunits within

Correspondence should be addressed to L.C. (linchen@usc.edu) or S.M.S. (sine@mayo.edu).
[5]These authors contributed equally to this work.

AUTHOR CONTRIBUTIONS

S.M.S. and L.C. supervised the project; S.H., N.B. and S.M.S. designed and built the α_7–AChBP chimera; N.B. and S.H. expressed the protein; S.H., N.B. and S.-X.L. purified the protein; S.-X.L., S.H., C.D.D., K.N. and L.C. grew the crystals; S.-X.L. and L.C. collected diffraction data, solved and refined the structure; S.M.S. and N.B. conducted the radioligand binding experiments; and S.M.S., L.C., S.L. and S.H. wrote the paper.

COMPETING FINANCIAL INTERESTS

The authors declare no competing financial interests.

Accession codes. RCSB Protein database: atomic coordinates and structure factors have been deposited with accession codes 3SQ9 (Apo) and 3SQ6 (Epi).

Note: Supplementary information is available on the Nature Neuroscience website.

the pentamer[1–3]. A cryoelectron microscopic structure of the *Torpedo marmorata* AChR disclosed the majority of the protein main chain and the approximate locations of residue side chains[4]. Further advances included X-ray crystal structures of the extracellular domain of the α_1 subunit from the muscle AChR bound to α-bungarotoxin[5], and of prokaryotic orthologs[6–8]. These advances provided key insights into AChR structure, yet an essential goal that remains is an X-ray crystal structure of an AChR from a eukaryotic source.

Neuronal nicotinic α_7 AChRs are abundant in many brain regions[9], notably in the hippocampus, where their pre- and postsynaptic locations[10] and high calcium permeability[11] suggest that they may contribute to learning and memory. α_7 AChRs exhibit distinctive pharmacology, with choline, a breakdown product of nerve-released acetylcholine (ACh), showing high efficacy[12], contrary to its low efficacy at muscle AChRs[13]. α_7 AChRs have been implicated in neuropsychiatric[14], neurodegenerative[15] and inflammatory[16] diseases, and thus are potential therapeutic targets for α_7-selective agonists or antagonists that could be designed on the basis of X-ray crystal structural data.

The homopentameric composition of α_7 AChRs confers advantages for structural studies. Furthermore, because the ligand-binding sites localize at interfaces between extracellular regions of the subunits[17], α_7 AChRs harbor five identical ligand-binding sites. Although the α_7 AChR and AChBP are homopentameric and share a similar structural fold, low sequence identity limits the use of AChBP structures for drug development and mechanistic studies.

For proteins that are difficult to express or crystallize, engineered protein modules provide valuable surrogates for structural analyses. A water-soluble α_7 ligand-binding domain was generated by truncating the protein chain before the first transmembrane domain, substituting the Cys-loop from AChBP and replacing hydrophobic with hydrophilic residues on the protein surface[18]. Here, we develop an analogous α_7–AChBP chimera and determine X-ray crystal structures of the resulting pentamer and its complex with the agonist epibatidine. The findings provide the highest resolution images yet of an AChR ligand-binding pocket, including structures that mediate ligand recognition, signal transduction and interaction with inorganic cations. Comparison of the structures reveals molecular rearrangements triggered by the agonist, enabling structure-guided mutational studies of the native α_7 AChR.

RESULTS

α_7–AChBP chimera construction and crystallographic analysis

The α_7 AChR extracellular domain failed to produce folded protein when expressed in yeast, whereas AChBP yielded milligram amounts of correctly folded protein. We therefore generated a series of chimeras, combining sequences from α_7 with those from AChBP, aiming to maximize α_7 sequences within secondary structures and important loop regions (Fig. 1 and Online Methods). The final construct shared 64% sequence identity and 71% similarity with native α_7 (Supplementary Fig. 1), was expressed in quantities similar to those of AChBP and eluted as a sharp peak on size exclusion chromatography with a retention volume similar to that of AChBP. The α_7–AChBP chimera bound radiolabeled α-bungarotoxin and epibatidine (Supplementary Fig. 2), suggesting that it is a good model for the ligand-binding domain of the α_7 AChR.

We crystallized the α_7–AChBP chimera in the absence of added ligands and in the presence of epibatidine, yielding Apo and Epi crystals, respectively. The Apo crystal diffracted to a resolution of 3.1 Å, and the Epi crystal diffracted to 2.8 Å. The higher resolution of the Epi crystal was probably due to stabilization by bound agonist. The Apo structure was solved by molecular replacement using AChBP (PDB code 1UW6) as the search model, and the Epi

structure was solved using the Apo structure as the search model. The Apo and Epi crystals shared a similar packing arrangement, with the asymmetric unit containing two nearly identical pentamers, one of which we describe below. For both crystals, the electron density maps were improved by tenfold non-crystallographic symmetry (NCS) averaging, which overcame partial data completeness in the highest resolution shells. The electron density maps were of high quality (Supplementary Figs. 3 and 4), enabling structural and mechanistic analyses. Statistics of data collection and structure refinement are listed in Supplementary Table 1.

Overall structure

The Apo form of the α_7–AChBP chimera has a canonical pentameric quaternary structure (Fig. 2a), which superimposes well on that of AChBP (Fig. 2b). Each monomer folds into a ten-stranded β-sandwich capped by an N-terminal α-helix (Supplementary Fig. 1b), as in AChBP and *Torpedo* AChR. The β-sandwich core of the chimera subunit can be superimposed on those of mouse α1 and AChBP (Fig. 2c), whereas the peripheral loops, α1–β1, β4–β5, β6–β7, and binding site loop F diverge, probably owing to sequence differences among the three proteins. The solvent-accessible surface consists of large and continuous regions of α_7 residues, including the ligand-binding site and structures that are implicated in signal transduction (Fig. 2d), whereas the Cys loop and a stripe within the central vestibule contain AChBP residues.

The subunit interface contains residues from α_7 and AChBP, yet the interface structures of the chimera and AChBP are similar. However, notable differences between the two structures are evident in the upper and lower parts of the interface. In the upper part, interactions between the α1–β1 loop from the principal face and the α1 helix and β2–β3 loop from the complementary face differ, probably owing to a buried hydrogen bond between Tyr14 and Asp60, conserved in AChRs but absent in AChBP, that links the α1–β1 and β2–β3 loops within each subunit (Supplementary Fig. 5). In the lower part, the β1–β2 loop from one subunit and loop F from the adjacent subunit show a local shift, probably owing to sequence differences (Supplementary Fig. 6). The Epi structure mirrors the Apo structure, except for the ligand-binding pocket and flanking regions (Fig. 2e). All ten binding sites in the asymmetric unit show electron density corresponding to an epibatidine molecule. Thus, in terms of the structural fold, surface properties and ligand-binding site, the Apo and Epi structures provide models for the native α_7 extracellular domain and conformational changes that are produced by agonists.

Ligand-binding pocket and flanking regions

The ligand-binding core and flanking regions are lined entirely by α_7 residues, providing structural bases to analyze principles of ligand recognition and signal transduction. Ligand recognition is accomplished by residues from loops A–C from the principal subunit and loops D–E from the complementary subunit, including Tyr91 from loop A, Trp145 from loop B, Tyr184 and Tyr191 from loop C, Trp53 from loop D, and Leu106, Gln114 and Leu116 from loop E. Within the binding pocket, residues that are conserved between the chimera and AChBP exhibit similar spatial arrangements, suggesting a generally conserved mode of ligand recognition (Supplementary Fig. 7). In muscle AChR, signal transduction is mediated by residues equivalent to Tyr184 from β-strand 9, Asp193 from β-strand 10 and Lys141 from β-strand 7 (ref. 19), which extend to the pore, enabling intra-subunit communication.

Regions that flank the ligand-binding core contain several α_7-specific residues of potential functional importance. These residues disperse around loop C, which changes conformation upon agonist binding[2,3] and initiates early steps in signal transduction[19,20]. Located in sub-

regions I–IV (Fig. 3a), these α_7-specific residues comprise Arg182 from loop C, which approaches Tyr184 and Lys141 of the same subunit (Fig. 3b and Supplementary Fig. 3a); Arg179 from loop C, which interacts with Asp153 from the β8–β9 loop and Glu181 from loop C of the same subunit (Fig. 3c); Glu185 from loop C, which approaches Glu158 and Asp160 from loop F of the complementary subunit (Fig. 3d,e); and a glycan from Asn108 of the complementary subunit that makes van der Waals contact with loop C of the principal subunit (Fig. 3f).

The Apo crystal showed a strong density at the center of the ligand-binding pocket (Supplementary Fig. 8). The chemical identity of this density is unknown, but its position overlapped with the quaternary ammonium moiety of carbamylcholine bound to AChBP (PDB 1UV6) and the alicyclic moiety of epibatidine in the Epi crystal.

Ligand-induced changes

Superposition of the Apo and Epi structures reveals changes in the ligand-binding pocket and surrounding regions (Fig. 2e), and these changes propagate to distal parts of the subunits and subunit interfaces (Fig. 4a). The most substantial change occurs in loop C, which in the Apo structure adopts a range of opened-up conformations among the different subunits (Fig. 4b). By contrast, in the Epi structure, loop C assumes a closed-in conformation in all ten subunits of the asymmetric unit. Given the conformational dynamics of loop C, NCS averaging was not applied to this region. Nevertheless, in the Apo and Epi structures, electron density for loop C is well defined (Supplementary Figs. 3a and 4a).

Smaller shifts are observed in loops α1–β1, A, B and F, and in β-strands 7, 9 and 10. These shifts comprise a concerted rotation of the outer β-sheet in a clockwise direction when viewed down an axis through the pentamer, while loops α1–β1, B and C rotate counterclockwise (Fig. 4a), altering the pentamer interface in this region (Supplementary Fig. 9). The rotation and twist of the outer sheet is accompanied by inward bending of the β-barrel, causing repacking of the β-sandwich core such that Phe196 switches between distinct rotamer positions (Fig. 4a,c); phenylalanine or tyrosine is present at the position equivalent to Phe196 in all AChR α-subunits. The concerted nature of these shifts suggests that they are not artifacts of limited resolution, which would produce random shifts. Moreover, the large change of Phe196 is clear at the current resolution (Fig. 4c). By contrast, the inner β-sheet remains stationary between the two structures (Fig. 4a).

Epibatidine-induced changes in loops A, B, C and F are accompanied by reorganization of residues within the ligand-binding pocket (Fig. 5a). The most substantial changes are shifts of Tyr184 of loop C and Tyr91 of loop A, which frame the tertiary nitrogen of epibati-dine against Trp145 from loop B. These primary stabilizing residues are augmented by Tyr191 from loop C and Trp53 from loop D, with Trp53 exhibiting multiple conformations in the Apo structure but only one conformation in the Epi structure. The positioning of the five conserved aromatic residues is similar to that noted for AChBP with bound epibatidine at 3.4 Å resolution[3] (Supplementary Fig. 7), but the 2.8 Å resolution of our Epi structure defines orientations of backbone carbonyls and aromatic side chains in a binding site containing solely α_7 residues.

In parallel with changes in the conserved aromatic residues, residues that are implicated in signal transduction rearrange and show previously unobserved interactions with ligand recognition residues (Fig. 5b). In the Apo structure, the Lys141 side chain is only partially defined by the electron density, suggesting dynamic motions or contacts among multiple partners. However, in the Epi structure the Lys141 side chain is defined, revealing a hydrogen bond between its ε-amino moiety and the aromatic hydroxyl of Tyr184 from loop C, and also a π–cation interaction with Tyr91 from loop A as it contacts epibatidine (Fig. 5c

and Supplementary Fig. 10). Furthermore, in the Apo structure, Arg182 exhibits two conformations, stacking against the aromatic ring of Tyr184 or extending toward Lys141 (Fig. 3b and Supplementary Fig. 3a), but in the Epi structure, Arg182 stacks uniformly against Tyr184 while simultaneously hydrogen bonding to the main-chain carbonyl of Phe183 and linking to Lys141 through a solvent molecule—most probably water (Fig. 5c and Supplementary Fig. 10). Thus, in the Apo structure, Tyr184, Tyr91, Lys141 and Arg182 disperse loosely within the binding site, but in the Epi structure they converge into an ordered assembly. Association of Lys141 with Tyr184 and Tyr91 was noted in the X-ray crystal structure of AChBP with bound nicotine[2], but not in that of AChBP with bound epibatidine[3]. With the addition of Arg182, our Epi structure reveals an ordered assembly of aromatic and cationic residues linking bound agonist to loop C, loop A and the base of the Cys-loop (Fig. 5c).

Additional α_7-specific residues that are associated with loop C may also be functionally important. In the Apo structure, Glu185 projects from the tip of loop C toward Glu158 and Asp160 from loop F of the opposing subunit, creating a region of negative electrostatic potential (Fig. 3e), while the glycan linked to Asn108 of the complementary subunit makes van der Waals contact with the disulfide bond between Cys186 and Cys187 from loop C of the principal subunit (Fig. 3f). In the Epi structure, the glycan dissociates from loop C as this loop clamps down on epibatidine (Fig. 5d), and loop F moves away from loop C, perhaps aided by repulsion between Glu185 and Glu158. In the Apo structure, the combination of a negative electrostatic potential and hydrophilic glycan may create an environment that facilitates the association of the cationic ACh or inorganic ion modulators such as calcium.

At the base of loop C, additional α_7-specific residues anchor loop C to loop F of the same subunit. In the Apo structure, Arg179 establishes electrostatic interaction with neighboring Glu181 and Asp153 from loop F, and it also hydrogen bonds to Gln155 from loop F (Fig. 3c). Asp153, in turn, hydrogen bonds to Thr28 from β-strand 1, while the aliphatic portion of Gln155 makes van der Waals contact with Tyr30. Van der Waals contacts also form between Met156 from loop F and main-chain atoms of Lys178 and Arg179. This network of surface-exposed residues, present in all subunits, is particularly well defined by the electron density maps. Positioned at the base of loop C, this stable network may act as a fulcrum against which loop C flexes. Indeed, in the higher resolution Epi structure, this network is maintained (Supplementary Fig. 11).

Epibatidine recognition and inter-subunit contacts

The azabicyclo moiety of epibatidine lodges in the center of the aromatic cage (Fig. 6). Stabilizing interactions comprise a π–cation interaction between the bridging amino group of epibatidine and the indole ring of Trp145, and hydrogen bonds between the bridging amino group and the main-chain carbonyl of Trp145 and the hydroxyl of Tyr91. These are augmented by extensive van der Waals contacts between the aliphatic portion of the azabicyclo moiety and Tyr184, Cys186, Cys187 and Trp145, and an interaction between the aromatic ring of Tyr191 and one of the two electropositive carbon atoms vicinal to the bridging amino group in epibatidine. The chloropyridine ring stacks edge-to-face against the indole ring of Trp145 and makes van der Waals contact with Thr146. At the complementary face of the binding site, the chlorine atom of epibatidine lodges close to the main-chain carbonyl groups of Gln114 (2.7 Å) and Leu104 (3.3 Å); the distances and geometry observed here concur with known halogen bonds, suggesting an unusual role in stabilizing epibatidine[21]. The chloropyridine ring also makes van der Waals contacts with Leu104, Leu106 and Gln114. Trp53 at the complementary face does not contact epibatidine directly, but stacks edge-to-face against Trp145, stabilizing that side chain. Comparing our Epi structure with AChBP bound to epibatidine[3] reveals a similar mode of ligand recognition mediated by a similar principal face but a divergent complementary face.

In native AChR, the ligand-binding domain establishes a major communication link with the pore domain[22,23]. In the present structures this linkage region exhibits previously unobserved inter-subunit interactions. The β1–β2 loops from adjacent subunits align in a head-to-tail manner, unlike in AChBP, in which successive β1–β2 loops make little contact (Fig. 7a). Lys44 from the tip of the β1–β2 loop of the principal subunit establishes electrostatic interaction with Asp40 from the tail of the β1–β2 loop of the complementary subunit, and Asn45 of the principal subunit hydrogen bonds with the main-chain carbonyl of Met39 of the complementary subunit. Asn45 is conserved among AChR α-subunits, but Lys44 and Asp40 are specific to certain neuronal AChRs (Fig. 1). Inter-subunit contacts that are mediated by the β1–β2 loops are augmented by interactions between β-strand 6 from the principal subunit and loops β1–β2 and F from the complementary subunit (Fig. 7b). For example, Ser124 in β-strand 6 of the principal subunit makes van der Waals contact with Ile165 in loop F and hydrogen bonds with Gln37 in the β1–β2 loop of the complementary subunit. In muscle AChR, residues that are equivalent to Ser124 and Gln37 mediate inter-subunit communication essential for efficient channel gating[24]. Moreover, the tandem arrangement of the β1–β2 loops creates a ring of ten aspartate and five asparagine residues that produces a strong negative surface potential facing the central vestibule, which in native α_7 AChRs may concentrate sodium and calcium ions for permeation.

Mutational analyses

The Epi structure suggested that primarily three residues from the principal face of the binding site stabilized epibatidine: Trp145 from loop B, Tyr184 from loop C and Tyr91 from loop A. To test this interpretation, we substituted phenylalanine for each of the five conserved aromatic residues in the α_7 AChR binding site and measured epibatidine binding. Under steady-state conditions, epibatidine bound to the α_7 AChR cooperatively and with high affinity (Fig. 8a). Substituting phenylalanine at any of the four positions at the principal face maintained cooperativity, whereas substituting at Trp53 at the complementary face markedly reduced cooperativity. Furthermore, phenylalanine substitutions increased the apparent dissociation constant by 4- to 2,200-fold, with the rank order Trp145 > Tyr184 > Tyr91 > Tyr191 > Trp53. Substitution at Trp145 reduces the size of the aromatic ring, which would weaken the π–cation interaction with the bridging nitrogen and the edge-to-face stacking with the chloropyridine ring on epibatidine, whereas substitution at Tyr91 would remove the hydrogen bond to the bridging nitrogen. Substitution at Tyr184 would remove the hydrogen bond to Lys141, impairing the closure of loop C and consequently weakening the π–cation interaction between Lys141 and Tyr91. Substitutions at Tyr191 and Trp53, however, decreased affinity to smaller extents. Thus, results from mutagenesis in α_7 are fully consistent with the model of epibatidine binding that is provided by our structure.

Measurements of steady-state agonist binding can also indicate changes in signal transduction. We therefore examined the binding of ACh to α_7 AChRs containing mutations of α_7-specific residues that were highlighted in the structures. Substitutions at Arg182, Glu185 and Glu181, all in loop C (Fig. 3), increased affinity of the agonist for the α_7 AChR (Fig. 8b). Substitution at Gln37, which spans the subunit interface (Fig. 7b), also increased affinity. Because ACh binding is highly cooperative, the observed increases in affinity show that agonist concentrations that minimally occupy native α_7 fully occupy the mutants. Steady-state agonist binding provides a global measure of AChR function, encompassing equilibria among resting, active and desensitized states and their associated affinities. Thus, these α_7-specific residues that are highlighted in the structures are likely to contribute to signal transduction steps linked to agonist binding.

DISCUSSION

Here we present X-ray crystal structures of a chimeric ligand- binding domain of the α_7 AChR in apo and agonist-bound conformations. Because the ligand-binding site and flanking regions consist entirely of α_7 residues, the structures provide the highest resolution images that have so far been obtained of the AChR in regions that govern ligand recognition and the initial steps in signal transduction. Furthermore, the structures provide realistic templates for computational drug design, as well as bases for probing structure–function relationships of the physiologically and clinically important neuronal α_7 AChR. The structures also resolve residues that emerge as candidates to confer α_7-specific functional properties. Among these, residues in loop C that do not contact bound agonist contribute to the inherently low agonist affinity of the α_7 AChR, suggesting that they affect transduction of agonist binding to channel gating or desensitization.

Within the ligand-binding cleft, conserved aromatic and α_7-specific residues stem from multiple canonical loops that form the ligand contact surface. Trp145 is the main stabilizing residue, as is evident from π–cation and dipole–cation interactions with the bridging nitrogen of epibatidine, and it exhibits the largest decrease in affinity on mutation. Trp145 shows little change between Apo- and Epi structures and thus is a stationary receiver to which agonist is directed by centric shifts of Tyr184 and Tyr91. The hydroxyl of Tyr91 from loop A directly stabilizes the bridging nitrogen on epibatidine, whereas the hydroxyl of Tyr184 provides little direct stabilization but stabilizes loop C in the closed-in conformation through interaction with Lys141 stemming from the base of the Cys-loop. Tyr91 and Tyr184 are further stabilized by π–cation interactions with Lys141 and Arg182, respectively. The convergence of these residues toward bound epibatidine creates an ordered assembly of cationic and aromatic side chains that locks loops A and C into positions that sequester the agonist.

Substituting phenylalanine for any of the five conserved aromatic residues reduced epibatidine affinity for the α_7 AChR, in accord with interactions that are seen in the bound complex. However, steady-state agonist binding is a composite measure, encompassing intrinsic affinity and signal transduction steps that are associated with resting, open channel and desensitized states. For example, in muscle AChR, substituting phenylalanine for the residue equivalent to Tyr184 decreases both agonist affinity and channel gating efficacy[20]. Analogously, in α_7, substituting phenylalanine for Tyr91 decreased affinity through loss of direct interaction with agonist, but it may also affect signal transduction through a change of the π–cation interaction with Lys141. Thus, although aromatic residues that contact agonist are clear in the Epi structure, their functional contributions are likely to encompass both agonist recognition and signal transduction.

Residues within the binding cleft unique to α_7 emerge as candidates to confer type-specific ligand recognition properties. At the principal face, the Pro190–Tyr191–Pro192 sequence in loop C, unique to α_7, α_9 and α_{10}, may affect interaction of Tyr191 with the agonist. At the complementary face, the ascending and descending β-strands of loop E offer a pair of main-chain carbonyl groups that engage in halogen bonding to the chlorine atom on epibatidine. This second anchor positions the chloropyridine ring to establish van der Waals contacts with loop E residues specific to α_7: Leu106, Leu116 and Glu114. Thus, toward computational drug design, our Epi structure provides the best available template because the binding site derives entirely from α_7 and the resolution is 2.8 Å.

Comparison of the Apo and Epi structures reveals changes within the ligand-binding pocket and flanking regions, highlighting the concept that ligand recognition not only draws together residues to stabilize agonist but also recruits residues to mediate signal

transduction. These local changes propagate to the rest of protein, leading to twisting, inward bending and repacking of the β-sandwich core of the subunit and the switching of Phe196 between distinct rotamer positions (Fig. 4a). The functional importance of these structural changes requires further study, but the present findings demonstrate that local changes due to agonist binding affect distal sites within the subunit and the pentamer.

Three α_7-specific residues in loop C—Arg182, Glu185 and Glu181—do not contact agonist but contribute to low affinity of the α_7 AChR. Mutation of any of these residues shifts steady-state ACh binding to lower concentrations; because agonist binding is cooperative, agonist concentrations that minimally occupy native α_7 fully occupy the mutant AChRs. Mechanistically, these residues may affect one or a combination of processes, including agonist affinity for resting, active or desensitized states, or transitions among these states. Arg182 and Glu185, located underneath loop C, juxtapose residues with the same charge, with Arg182 pairing with Lys141 and Glu185 pairing with Glu158 and Asp160. The increased affinity produced by the mutants R182V and E185Q may thus arise from relief of electrostatic repulsion, which in native α_7 may favor the opened-up conformation of loop C, contributing to low agonist affinity. On the other side of loop C, Glu181 is part of a network encompassing Arg179, Asp 153 and Gln155, anchoring loop C to loop F. In native α_7, this network may promote low agonist affinity, as disrupting it with the mutation E181S increases affinity. Thus, by revealing inter-residue interactions of α_7-specific residues, the present structures provide insights into the unique functional properties of α_7 AChRs.

The structures exhibit a tandem arrangement of β1–β2 loops that creates a ring of ten aspartate and five asparagine residues facing the central vestibule that may concentrate cations before translocation. This arrangement arises through extensive inter-subunit contacts, comprising van der Waals, hydrogen bonding and electrostatic forces between successive β1–β2 loops and between β4–β5 and Cys loops of one subunit and loop F of the opposing subunit. In muscle AChR, simulations of single-cation translocation showed discrete pauses of the cation, one of which coincided with the ring identified here[25]. However, in muscle AChR, the ring contains five fewer Asp residues, perhaps contributing to its lower unitary conductance and reduced calcium permeability. In the recent structure of a glutamate-activated chloride channel from the Cys-loop superfamily[26], this ring is neutral, containing lysine, aspartate and asparagine at equivalent positions, in line with its anion selectivity. Thus, the present findings not only define structures conserved among AChRs but also structures unique to α_7.

ONLINE METHODS

Construction of the α_7–AChBP chimera

The initial cDNA construct, cloned into the yeast vector pPICZαA (Invitrogen), comprised segments encoding the AChBP sequence[27] from the N terminus through the signature Cys loop followed by the human α_7 sequence (GenBank accession number X70297) to the C-terminal end of the extracellular domain and an M2 Flag affinity tag. This construct expressed poorly, but addition of three segments of AChBP sequence ($_{146}$THHSR$_{150}$, $_{167}$YSRF$_{170}$, $_{175}$VTQ$_{177}$) afforded abundant α-bungarotoxin binding and yielded pentameric protein on size exclusion chromatography. To increase the proportion of α_7 sequence, segments of α_7 were substituted successively into individual secondary structures and loop regions using combinations of inverse polymerase chain reaction (PCR) and homologous recombination[28], and overlap extension PCR[29], followed by assessment of α-bungarotoxin binding[30] and pentamer formation[31]. The final construct, confirmed by sequencing, bound quantities of α-bungarotoxin similar to those bound by AChBP, and on size exclusion chromatography eluted with a slightly longer retention time than AChBP.

Protein expression

The α_7–AChBP chimera cDNA was digested with SacI, and introduced into *Pichia pastoris* strain KM71H (Invitrogen) by electroporation. The transformed yeast were applied to plates containing YPDS growth medium supplemented with zeocin (1 mg ml^{-1}), and after 3 d at 30 °C, colonies were picked and seeded into small-scale cultures of BMGY medium, followed by BMMY medium for expression. Cell suspensions were centrifuged and supernatants analyzed for protein expression by chemiluminescence (Roche) based on the M2 Flag tag. The colony with the highest protein yield was seeded into a 50-ml culture placed into a rotary shaker overnight at 30 °C and then added to 5 liters of BMGY medium that was shaken at 30 °C until the OD_{600} reached a value of between 2 and 4. The cell suspension was centrifuged at 2,000*g* for 5 min at 22–24 °C and resuspended in 1 liter of BMMY medium to induce expression. After induction for 3 d, with addition of methanol (0.5 % vol/vol) every 24 h, culture supernatants were collected for purification.

Protein purification

The culture supernatant was applied to an anti-Flag M2 agarose affinity gel (Sigma), and protein was eluted using an M2 Flag peptide at 0.1 mM in 50 mM potassium phosphate buffer, 0.15 M NaCl, pH 6.0. Eluted protein was further purified by size exclusion chromatography (Superdex 200 10/300 GL, GE) using a Biologic Duoflow system (Bio-Rad) and isocratic elution with 50 mM potassium phosphate, 0.15 M NaCl, pH 6.0. Protein fractions were identified by OD_{280}, pooled and concentrated for analysis and crystallization. Although the final protein exhibited differential glycosylation on SDS gels, multi-angle light scattering showed predominantly monodisperse protein. We therefore used the glycosylated protein for crystallization.

Crystallization, data collection and structure determination

Both the Apo α_7–AChBP chimera and Epi chimera complex crystals were grown at 18–24 °C using the hanging-drop vapor diffusion method by mixing protein (5.3 mg ml^{-1}, 1–2 μl) with an equal volume of reservoir solution. For the Apo chimera crystallization, the well solution contained 0.1 M Bis–Tris, pH 6.5, 20% PEGMME 2000, 0.2% NaN_3. Plate-like crystals appeared overnight and reached dimensions of ~0.2 × 0.2 × 0.02 mm^3 in 4–5 d. Only 1%–2% of crystals were suitable for data collection owing to high mosaicity. For the Epi chimera complex crystallization, epibatidine and protein were mixed at a molar ratio of ~10:1 and then the sample was incubated on ice for 1.5 h. The crystals were grown in 0.1 M Tris–HCl, pH 8.0, 18% PEGMME2K, 0.2 M trimethylamine *N*-oxide dehydrate, 0.2% NaN_3.

Data were collected at the ALS beamline 8.2.2 at Lawrence Berkeley National Laboratory at 100 °K. Before flashing cooling, crystals were equilibrated for 10–20 s in cryoprotectant buffer containing mother liquor with 10% glycerol. Data were processed and scaled using HKL2000 (ref. 32). Both Apo chimera and Epi chimera complex crystals belong to the space group $P2_1$, with unit cell dimensions a = 79.126 Å, b = 144.564 Å, c = 131.114 Å, β = 102.45°; and a = 81.237 Å, b = 141.069 Å, c = 130.207 Å, β = 99.649°, respectively. For both crystals, there were two pentamers in each asymmetric unit. The Apo structure was solved by molecular replacement with the program Molrep[33] using AChBP (PDB: 1UW6)[2] as the search model. The model for the crystal structure was rebuilt using Coot[34] and refined with CNS[35]. An NCS restraint was used to improve refinement, excluding residues in loop C (Arg179 through to Asp193) and the ligand-binding pocket. The same methods were used to determine Epi chimera complex structure except using the refined Apo structure as the search model. All maps are σ-A weighted. Crystallographic analysis and refinement statistics are summarized in Supplementary Table 1. Because chains D and E of the Apo

structure showed the most open conformation of loop C, they are used as the reference structure to compare the Apo and Epi structures in Figure 4a.

Ligand-binding measurements to wild type and mutant α_7 AChRs

cDNAs encoding the human α_7 AChR and RIC3 (ref. 36) were cotransfected into 293 HEK cells as described previously[37]. Mutations of the α_7 AChR were generated using QuikChange (Stratagene), followed by sequencing of the entire coding region. Binding of ACh or epibatidine to intact cells in suspension was measured by competition against the initial rate of ^{125}I-labeled α-bungarotoxin (PerkinElmer) binding as described previously[38].

Supplementary Material

Refer to Web version on PubMed Central for supplementary material.

Acknowledgments

We thank Advanced Light Source Berkeley Center for Structural Biology staff members C. Ralston, P. Zwart, C. Bertoldo, A. Rozales and K. Royal for help with data collection, N. Chelyapov and University of Southern California NanoBiophysics Core Facility for help with multi-angle light scattering analyses and P. Taylor for providing cDNA encoding AChBP. This work is supported by US National Institutes of Health grants NS031744 to S.M.S. and HL076334 and GM064642 to L.C.

References

1. Brejc K, et al. Crystal structure of an ACh-binding protein reveals the ligand-binding domain of nicotinic receptors. Nature. 2001; 411:269–276. [PubMed: 11357122]
2. Celie PH, et al. Nicotine and carbamylcholine binding to nicotinic acetylcholine receptors as studied in AChBP crystal structures. Neuron. 2004; 41:907–914. [PubMed: 15046723]
3. Hansen SB, et al. Structures of Aplysia AChBP complexes with nicotinic agonists and antagonists reveal distinctive binding interfaces and conformations. EMBO J. 2005; 24:3635–3646. [PubMed: 16193063]
4. Unwin N. Refined structure of the nicotinic receptor at 4 Å resolution. J Mol Biol. 2005; 346:967–989. [PubMed: 15701510]
5. Dellisanti CD, Yao Y, Stroud JC, Wang ZZ, Chen L. Crystal structure of the extracellular domain of nAChR α1 bound to alpha-bungarotoxin at 1.94 Å resolution. Nat Neurosci. 2007; 10:953–962. [PubMed: 17643119]
6. Hilf RJ, Dutzler R. X-ray structure of a prokaryotic pentameric ligand-gated ion channel. Nature. 2008; 452:375–379. [PubMed: 18322461]
7. Hilf RJ, Dutzler R. Structure of a potentially open state of a proton-activated pentameric ligand-gated ion channel. Nature. 2009; 457:115–118. [PubMed: 18987630]
8. Bocquet N, et al. X-ray structure of a pentameric ligand-gated ion channel in an apparently open conformation. Nature. 2009; 457:111–114. [PubMed: 18987633]
9. Breese CR, et al. Comparison of regional expression of nicotinic acetylcholine receptor α7 mRNA and [^{125}I]-α-bungarotoxin binding in human postmortem brain. J Comp Neurol. 1997; 387:385–398. [PubMed: 9335422]
10. Fabian-Fine R, et al. Ultrastructural distribution of the α 7 nicotinic acetylcholine receptor subunit in rat hippocampus. J Neurosci. 2001; 21:7993–8003. [PubMed: 11588172]
11. Seguéla P, Wadiche J, Dinely-Miller K, Dani J, Patrick JW. Molecular cloning, functional properties, and distribution of rat brain alpha 7: a nicotinic cation channel highly permeable to calcium. J Neurosci. 1993; 13:596–604. [PubMed: 7678857]
12. Alkondon M, Pereira EF, Cortes WS, Maelicke A, Albuquerque EX. Choline is a selective agonist of alpha7 nicotinic acetylcholine receptors in the rat brain neurons. Eur J Neurosci. 1997; 9:2734–2742. [PubMed: 9517478]

13. Grosman C, Auerbach A. Asymmetric and independent contribution of the second transmembrane segment 12′ residues to diliganded gating of acetylcholine receptor single channels: a single channel study with choline as the agonist. J Gen Physiol. 2000; 115:637–651. [PubMed: 10779320]
14. Martin LF, Kem WR, Freedman R. Alpha-7 nicotinic receptor agonists: potential new candidates for the treatment of schizophrenia. Psychopharmacology. 2004; 174:54–64. [PubMed: 15205879]
15. D'Andrea MR, Nagele RG. Targeting the alpha-7 nicotinic acetylcholine receptor to reduce amyloid accumulation in Alzheimer's disease pyramidal neurons. Curr Pharm Des. 2006; 12:677–684. [PubMed: 16472157]
16. Wang H, et al. Nicotinic acetylcholine receptor a7 subunit is an essential regulator of inflammation. Nature. 2003; 421:384–388. [PubMed: 12508119]
17. Sine SM. The nicotinic receptor ligand binding domain. J Neurobiol. 2002; 53:431–446. [PubMed: 12436411]
18. Zouridakis M, Zisimopoulou P, Eliopoulos E, Poulas K, Tzartos SJ. Design and expression of human alpha7 nicotinic acetylcholine receptor extracellular domain mutants with enhanced solubility and ligand-binding properties. Biochim Biophys Acta. 2009; 1794:355–366. [PubMed: 19059502]
19. Mukhtasimova N, Free C, Sine SM. Initial coupling of binding to gating mediated by conserved residues in muscle nicotinic receptor. J Gen Physiol. 2005; 126:23–39. [PubMed: 15955875]
20. Grosman C, Zhou M, Auerbach A. Mapping the conformational wave of acetylcholine receptor channel gating. Nature. 2000; 403:773–776. [PubMed: 10693806]
21. Metrangolo P, Neukirch H, Pilati T, Resnati G. Halogen bonding based recognition processes: A world parallel to hydrogen bonding. Acc Chem Res. 2005; 38:386–395. [PubMed: 15895976]
22. Bouzat C, et al. Coupling of agonist binding to channel gating in an ACh-binding protein linked to an ion channel. Nature. 2004; 430:896–900. [PubMed: 15318223]
23. Lee WY, Sine SM. Principal pathway coupling agonist binding to channel gating in the nicotinic receptor. Nature. 2005; 438:243–247. [PubMed: 16281039]
24. Mukhtasimova N, Sine SM. An inter-subunit trigger of channel gating in the muscle nicotinic receptor. J Neurosci. 2007; 27:4110–4119. [PubMed: 17428989]
25. Wang HL, Cheng X, Taylor P, McCammon JA, Sine SM. Control of cation permeation through the nicotinic receptor channel. PLoS Comput Biol. 2008; 4:e41, 1–9. [PubMed: 18282090]
26. Hibbs RE, Gouaux E. Principles of activation and permeation in an anion-selective Cys-loop receptor. Nature. 2011; 474:54–60. [PubMed: 21572436]
27. Smit AB, et al. A glia-derived acetylcholine-binding protein that modulates synaptic transmission. Nature. 2001; 411:261–268. [PubMed: 11357121]
28. Jones DH, Winistorfer SC. Recombinant circle PCR and recombination PCR for site-specific mutagenesis without PCR product purification. Biotechniques. 1992; 12:528–530. [PubMed: 1503755]
29. Heckman KL, Pease LR. Gene splicing and mutagenesis by PCR-driven overlap extension. Nat Protoc. 2007; 2:924–932. [PubMed: 17446874]
30. Gao F, et al. Curariform antagonists bind in different orientations to acetylcholine binding protein. J Biol Chem. 2003; 278:23020–23026. [PubMed: 12682067]
31. Gao F, et al. Solution NMR of acetylcholine binding protein reveals agonist-mediated conformational change of the C-loop. Mol Pharmacol. 2006; 70:1230–1235. [PubMed: 16847142]
32. Otwinowski Z, Minor W. Processing of X-ray diffraction data collected in oscillation mode. Methods Enzymol. 1997; 276:307–326.
33. Vagin A, Teplyakov A. Molecular replacement with MOLREP. Acta Crystallogr D Biol Crystallogr. 2010; 66:22–25. [PubMed: 20057045]
34. Emsley P, et al. Features and development of Coot. Acta Crystallogr D Biol Crystallogr. 2010; 66:486–501. [PubMed: 20383002]
35. Brünger AT, et al. Crystallography & NMR system: A new software suite for macromolecular structure determination. Acta Crystallogr D Biol Crystallogr. 1998; 54:905–921. [PubMed: 9757107]

36. Williams ME, et al. Ric-3 promotes functional expression of the nicotinic acetylcholine receptor alpha7 subunit in mammalian cells. J Biol Chem. 2005; 280:1257–1263. [PubMed: 15504725]

37. Bouzat C, Bartos M, Corradi J, Sine SM. Binding-pore interface of homomeric Cys-loop receptors governs open channel lifetime and rate of desensitization. J Neurosci. 2008; 28:7808–7819. [PubMed: 18667613]

38. Sine SM, Quiram P, Papanikolaou F, Kreienkamp HJ, Taylor P. Conserved tyrosines in the α subunit of the nicotinic acetylcholine receptor stabilize quaternary ammonium groups of agonists and curariform antagonists. J Biol Chem. 1994; 269:8808–8816. [PubMed: 8132615]

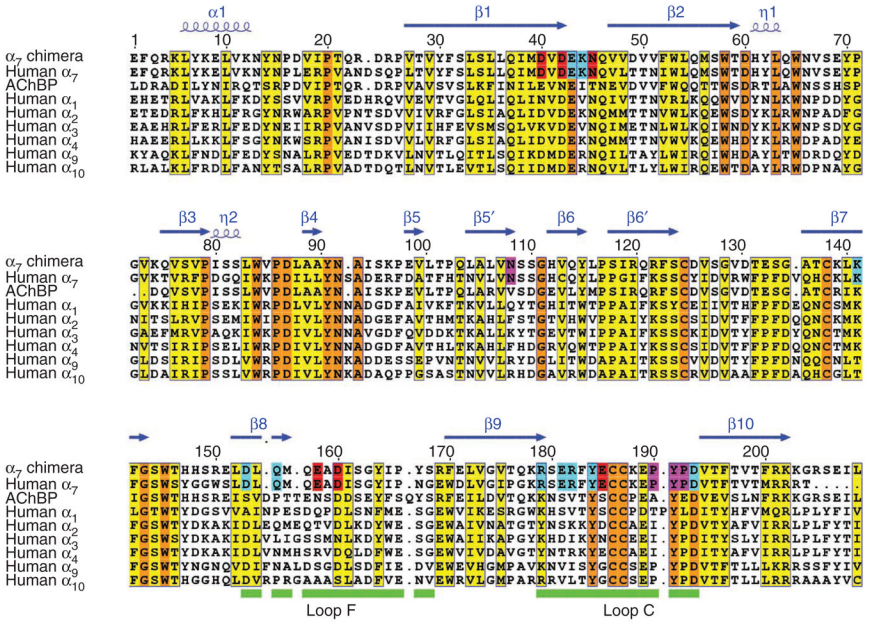

Figure 1.

Sequence and numbering of the α_7–AChBP chimera and its alignment with related AChR sequences. Orange indicates invariant residues and yellow indicates partially conserved residues. Secondary structures are shown schematically above the sequences. Putative functionally important residues for ligand recognition (pink), signal transduction (blue) and inorganic ion binding (red) are shown. Loops F and C are indicated by green bars.

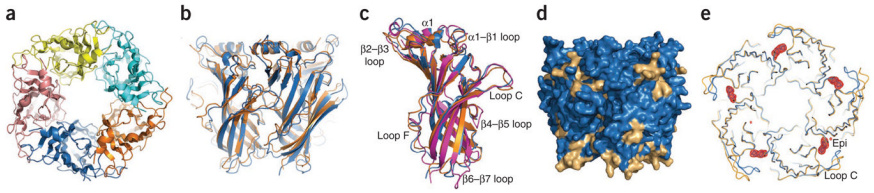

Figure 2.

Overall structures of the α_7–AChBP chimera and comparison to related structures. (**a**) Top view of the α_7–AChBP chimera pentamer along the five-fold axis of symmetry; each subunit is shown in a different color. (**b**) Structure superposition between the α_7–AChBP chimera (blue) and AChBP (orange) pentamers viewed from the side that is normal to the five-fold axis. (**c**) Structure superposition of subunits from the α_7–AChBP chimera (blue), α_1 extracellular domain (magenta) and AChBP (orange); loops showing substantial differences are labeled. (**d**) Surface representation showing α_7 residues (blue) and AChBP residues area (beige) on the α_7–AChBP chimera. (**e**) Backbone superposition between the Apo (gold) and Epi (blue) structures viewed down the five-fold axis. The epibatidine molecule (Epi) is shown by the $Fo - Fc$ electron density contoured at the 3.0-σ level.

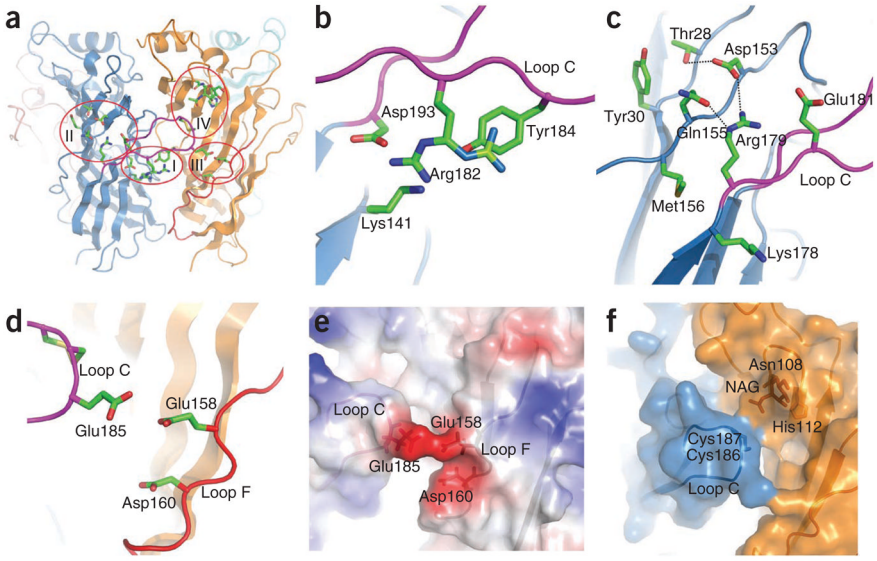

Figure 3.

Structures specific to α_7 revealed by the α_7–AChBP chimera. (**a**) Four regions of α_7-specific residues near loops C (magenta) and F (red), indicated by I–IV. (**b**) Close-up of the signal transduction region beneath loop C. Alternative conformations of Arg182 are indicated by different colors. (**c**) Close-up of linkage region between loops C and F within the same subunit. (**d**,**e**) Glu185-Glu158-Asp160 triad spanning loop C of the principal subunit and loop F of the complementary subunit, in ribbon (**d**) and surface (**e**) representation. Positive and negative surface potentials are indicated by blue and red, respectively. (**f**) Close-up of glycan across from loop C. NAG, *N*-acetylglucosamine.

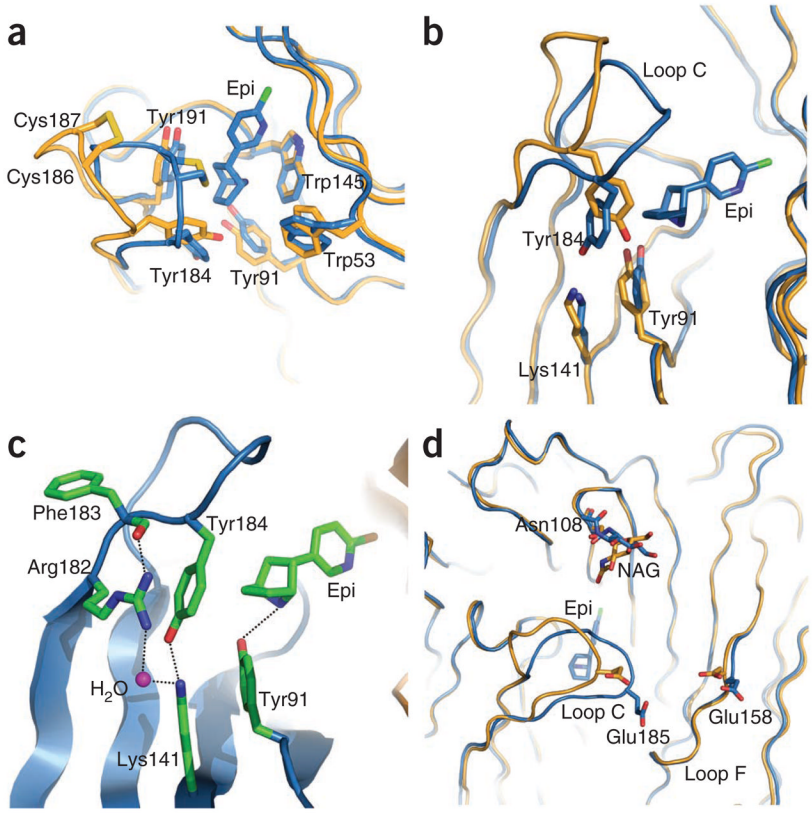

Figure 4.

Epibatidine-induced conformational changes. (**a**) Backbone superposition between the Apo (gold) and Epi (blue) structures shows a clockwise rotation of the outer β-sheet (green box and arrow, bottom) and a counterclockwise rotation of the top part of the subunit structure (red box and arrow, top) when viewed down the pentamer axis. The stationary inner sheet is indicated by the black box, and the epibatidine molecule is shown in electron density. The side chain rotamer switch of Phe196 is also evident in the green box. (**b**) Backbone superposition of individual subunits show variable conformations of loop C in the Apo structure (ten subunits colored differently) but a single closed conformation in the Epi structure (black, only one structure shown). Epi indicates the epibatidine molecule. (**c**) The $2Fo - Fc$ electron density map (contoured at the 1.0-σ level) shows the distinct side chain conformations of Phe196 (arrows) in the Apo (left) and Epi (right) structures, demonstrating repacking of the protein core as a result of epibatidine-induced structural changes.

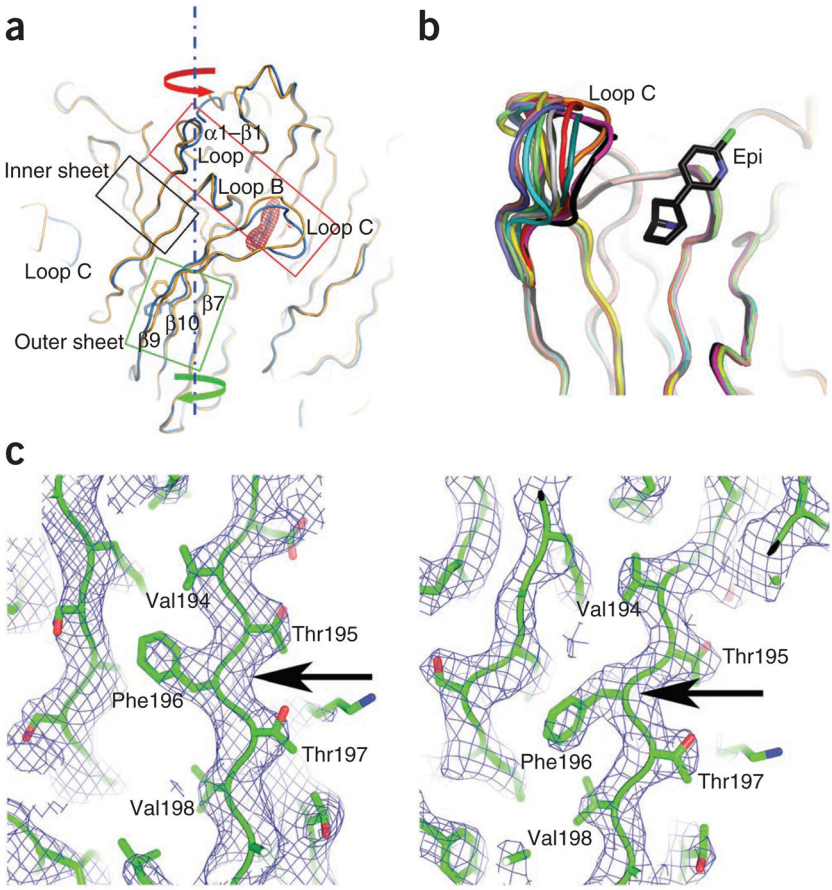

Figure 5.

Epibatidine-induced structural reorganization of the ligand-binding pocket and flanking regions. (**a**) Comparison of the ligand-binding pocket between the Apo (gold) and Epi (blue) structures. (**b**) Comparison of key residues underneath loop C implicated in signal transduction. (**c**) Highly ordered assembly of Tyr184, Tyr91, Lys141, Arg182 and a solvent molecule in the Epi structure. Epi indicates the epibatidine molecule. (**d**) Comparison of the interactions at the tip of loop C between the Apo (gold) and Epi (blue) structures. NAG, *N*-acetylglucosamine.

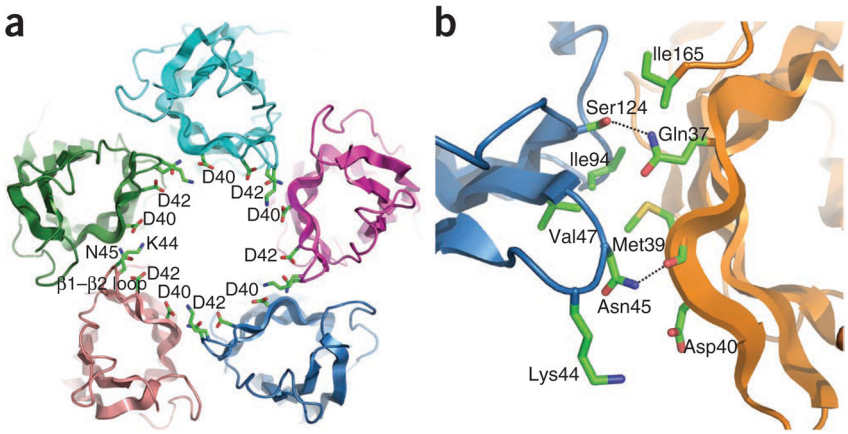

Figure 6.

Molecular recognition of epibatidine. (**a**) Stereo view of the ligand-binding pocket from the side of the pentamer showing the position of epibatidine (Epi) in the aromatic cage. The protein is in ribbon style and the epibatidine molecule is shown with the *Fo* – *Fc* electron density contoured at the 3.0-σ level. (**b**) Stereo view of the ligand-binding pocket from above the pentamer. This view highlights hydrogen-bond interactions and interactions with the complementary face of the binding site between epibatidine and the receptor chimera.

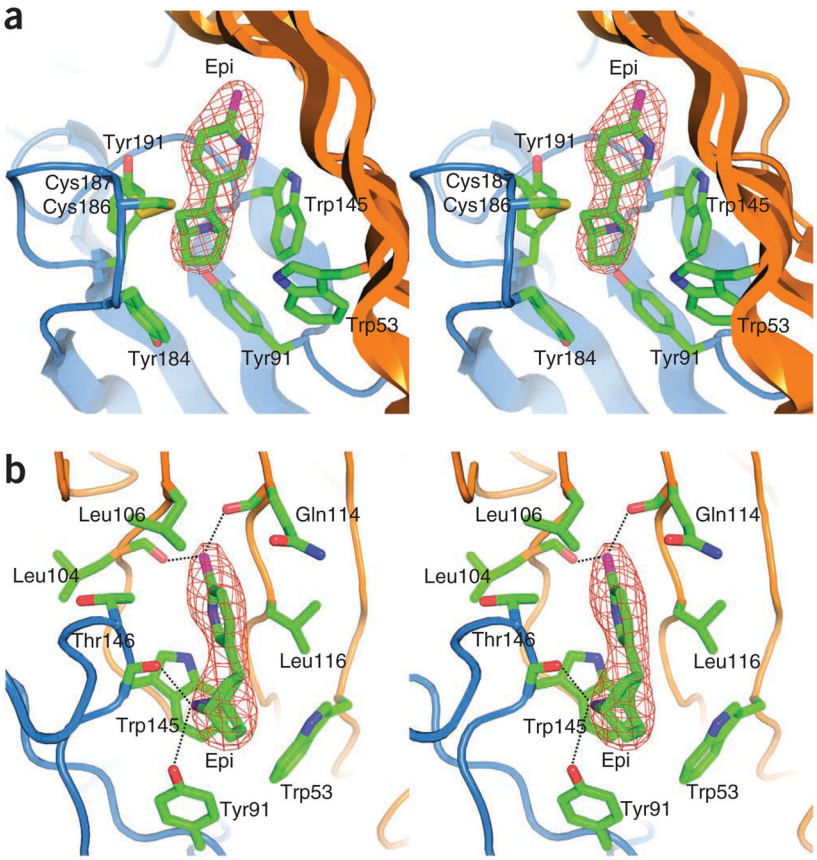

Figure 7.

Pore-facing regions of inter-subunit contact. (**a**) Bottom view of the pentamer along the five-fold axis of symmetry, showing the tandem arrangement of the β1–β2 loops and the ring of ten aspartate and five asparagine residues. (**b**) Inter-subunit contacts between the tip of the β1–β2 loop of the principal subunit (blue) and the stem of the β1–β2 loop of the complementary subunit (orange).

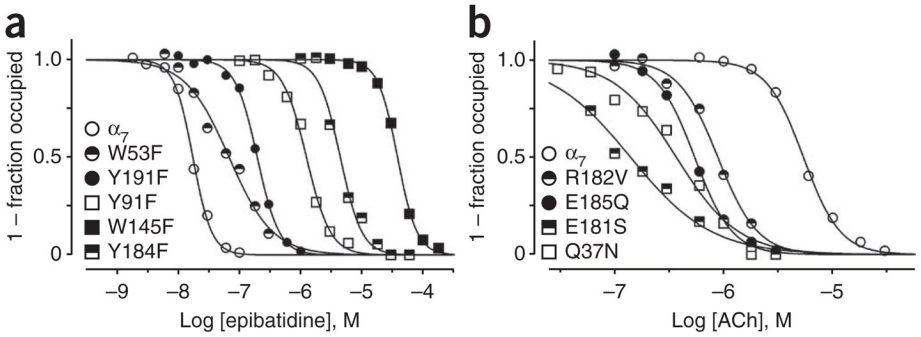

Figure 8.

Agonist binding after mutation of key residues. (**a**) Ligand contact residues. (**b**) Non-contact residues. Binding of epibatidine and ACh to native α_7 AChRs was measured by competition against the initial rate of ^{125}I-labeled α-bungarotoxin binding (see Online Methods). Curves are nonlinear least-squares fits of the Hill equation to the data with fit parameters given in Supplementary Table 2.